Biology of Reproduction, 2020, 102(2), 434–444
doi:10.1093/biolre/ioz181
Research Article
Advance Access Publication Date: 12 September 2019

OXFORD

Research Article

Impact of ferumoxytol magnetic resonance imaging on the rhesus macaque maternal–fetal interface†

Sydney M. Nguyen[1,2], Gregory J. Wiepz[1], Michele Schotzko[1], Heather A. Simmons[1], Andres Mejia[1], Kai D. Ludwig[3], Ante Zhu[4,5], Kevin Brunner[1,6], Diego Hernando[3,5], Scott B. Reeder[3,4,5,6,7], Oliver Wieben[3,5], Kevin Johnson[3,5], Dinesh Shah[2] and Thaddeus G. Golos[1,2,8,*]

[1]Wisconsin National Primate Research Center (WNPRC), Madison, Wisconsin, USA [2]Obstetrics & Gynecology, University of Wisconsin Madison School of Medicine, Madison, Wisconsin, USA [3]Medical Physics, University of Wisconsin Madison, Madison, Wisconsin, USA [4]Biomedical Engineering, University of Wisconsin Madison, Madison, Wisconsin, USA [5]Radiology, University of Wisconsin Madison, Madison, Wisconsin, USA [6]Emergency Medicine, University of Wisconsin Madison, Madison, Wisconsin, USA [7]Medicine, University of Wisconsin Madison, Madison, Wisconsin, USA, and [8]Comparative Biosciences, University of Wisconsin Madison, Madison, Wisconsin, USA

***Correspondence:** 1223 Capitol CT. Madison, Wisconsin 53715-1299, USA. Tel: 608-263-3567; E-mail: golos@primate.wisc.edu

†Grant Support: The National Institutes of Health (NIH) Grants U01HD087216 to D. Shah and O. Wieben, University of Wisconsin Institute for Clinical and Translational Research (UW ICTR) UL1 TR000427 (to M. Drezner), TL1 TR000429 (to KDL), UW Radiological Sciences Training Grant T32 CA009206 (to KDL), K24 DK102595 (to SBR), R01 DK011651 (to SBR), R01 DK117354 (to DH), Endocrinology-Reproductive Physiology Training Grant T32 HD041921 (to SMN), and P51 OD011106 (to the WNPRC).

Received 3 June 2019; Revised 5 August 2019; Accepted 3 September 2019

Abstract

Ferumoxytol is a superparamagnetic iron oxide nanoparticle used off-label as an intravascular magnetic resonance imaging (MRI) contrast agent. Additionally, ferumoxytol-uptake by macrophages facilitates detection of inflammatory sites by MRI through ferumoxytol-induced image contrast changes. Therefore, ferumoxytol-enhanced MRI holds great potential for assessing vascular function and inflammatory response, critical to determine placental health in pregnancy. This study sought to assess the fetoplacental unit and selected maternal tissues, pregnancy outcomes, and fetal well-being after ferumoxytol administration. In initial developmental studies, seven pregnant rhesus macaques were imaged with or without ferumoxytol administration. Pregnancies went to term with vaginal delivery and infants showed normal growth rates compared to control animals born the same year that did not undergo MRI. To determine the impact of ferumoxytol on the maternal–fetal interface (MFI), fetal well-being, and pregnancy outcome, four pregnant rhesus macaques at ~100 gestational day underwent MRI before and after ferumoxytol administration. Collection of the fetoplacental unit and selected maternal tissues was performed 2–3 days following ferumoxytol administration. A control group that did not receive ferumoxytol or MRI was used for comparison. Iron levels in fetal and MFI tissues did not differ between groups,

and there was no significant difference in tissue histopathology with or without exposure to ferumoxytol, and no effect on placental hormone secretion. Together, these results suggest that the use of ferumoxytol and MRI in pregnant rhesus macaques does not negatively impact the MFI and can be a valuable experimental tool in research with this important animal model.

Summary Sentence

Ferumoxytol magnetic resonance imaging for non-invasive pregnancy monitoring of the rhesus macaque does not impact histopathology or iron content of the maternal–fetal interface.

Key words: ferumoxytol, imaging, iron nanoparticles, MRI, placenta, pregnancy, primates

Introduction

In the hemochorial human and non-human primate placenta, maternal intervillous blood bathes the placental villi, allowing oxygen and nutrient transfer to the fetal blood circulating within the capillaries of the villous stroma. Pregnancy complications may stem from maladaptation of maternal vessels causing insufficient placental perfusion, leading to macrophage recruitment, cytokine release, and hypoxia at the maternal–fetal interface (MFI). Compromised intervillous flow is associated with adverse pregnancy outcomes [1–4]: insufficient placental perfusion could result in fetal growth restriction, preeclampsia, and pregnancy loss. The ability to identify abnormal uteroplacental vascular adaptation, compromised perfusion, and attendant inflammation could be valuable in identifying at-risk pregnancies before clinical manifestations.

Currently, ultrasound is the most commonly used method to assess fetal growth. It is also used to detect umbilical and uteroplacental blood flow abnormalities, but only indirectly through velocity waveform analysis. Further, ultrasound lacks the ability to detect immune cell homing to the MFI that may precede adverse pregnancy outcomes. Magnetic resonance imaging (MRI) can provide high-resolution anatomic and functional information including blood velocities and flow, perfusion, and oxygenation to characterize placental implantation site, visualize maternal pelvic structures, and diagnose abnormally aggressive trophoblast invasion or placental abruption [5]. In many clinical applications, gadolinium-based contrast agents (GBCAs) are used to quantify tissue perfusion and perform high-resolution angiography [6]. In the non-human primate, gadolinium MRI has been used to investigate spiral artery and perfusion domain (cotyledon) location, and quantify placental perfusion [7, 8], the latter of which has also been achieved in humans [9]. However, GBCAs have been shown to cross the placenta into the fetus with uncertainty in the long-term consequences of in utero GBCA exposure [10]. Although there is no specific evidence that it causes teratogenic or chromosomal damage [11–13], the risk to the fetus of gadolinium-based MR contrast agent administration remains unknown and should not be routinely provided to pregnant patients [14].

In this study, we explored an alternative approach for quantitative tissue perfusion and MR angiography in pregnancy, using the superparamagnetic iron oxide nanoparticle (SPION) ferumoxytol as a contrast agent. Ferumoxytol is approved by the Federal Drug Administration (FDA) for the treatment of anemia in adults with renal insufficiency and for iron deficiency anemias refractory to oral iron therapy [15]. It is considered to be safe and effective for treatment of iron deficiency anemia refractory to oral iron therapy in pregnant women [16]. Ferumoxytol has also emerged as an off-label MR contrast agent at a much lower dose than is used therapeutically for anemia. Ferumoxytol has favorable MR properties [17, 18] that can yield high-detail angiography and functional information about the MFI non-invasively, including quantitative perfusion maps of maternal blood that allow for analysis of individual cotyledons in the placenta [19], as seen in imaging with gadolinium [7]. As such, it has high potential to identify local and global perfusion abnormalities that might be indicative of placenta pathologies. Ferumoxytol also has the potential to spatially localize inflammatory events, as the nanoparticles are taken up by activated cells of the mononuclear phagocyte system at sites of tissue inflammation, which can then be imaged after ferumoxytol in the blood space has cleared [17, 20–24]. The MRI transverse relaxation rate R2* has a relationship with the concentration of iron in tissue. Therefore, R2* mapping may enable localization of iron-laden macrophages, as well as quantification of their density. Ferumoxytol's safety profile and properties for MR imaging make it a promising contrast agent to address the unmet need for non-invasive diagnosis of placental health with potential for clinical routine use. Importantly, demonstrating its use for placental imaging is a necessary step in this application. Therefore, the purpose of this work was to assess the feasibility of ferumoxytol imaging and the impact of administration on the MFI, fetal well-being, and pregnancy outcomes in a non-human primate model. The rhesus macaque provides an accurate experimental model of the human MFI and immune system, having hemochorial placentation, endovascular trophoblast invasion with attendant spiral artery remodeling, and chorionic villous placental architecture.

Materials and methods

Ethics statement

This study was approved by the University of Wisconsin-Madison Graduate School Institutional Animal Care and Use Committee. Twelve pregnant macaques in the WNPRC breeding colony were used for peripheral blood mononuclear cell (PBMC) experiments, placentas from six macaques from unrelated projects were used for placenta explant experiments, four pregnant macaques were imaged by MRI without ferumoxytol, and seven pregnant macaques were imaged by MRI with ferumoxytol, four of which ended in fetectomy. An additional four pregnant macaques went to fetectomy without imaging.

Care and use of macaques

Female rhesus macaques in the Wisconsin National Primate Center (WNPRC) breeding colony were housed with compatible males and monitored for breeding and menses. Pregnancies were confirmed and dated (+/−2 days) based on menstrual cycle, observation of copulation, and ultrasound measurements of gestational sac and fetuses. Blood samples were collected using a needle and syringe or vacutainer system from the femoral or saphenous vein. All infants born from this study (i.e., were not taken by fetectomy) joined the WNPRC colony. All macaques were cared for by WNPRC

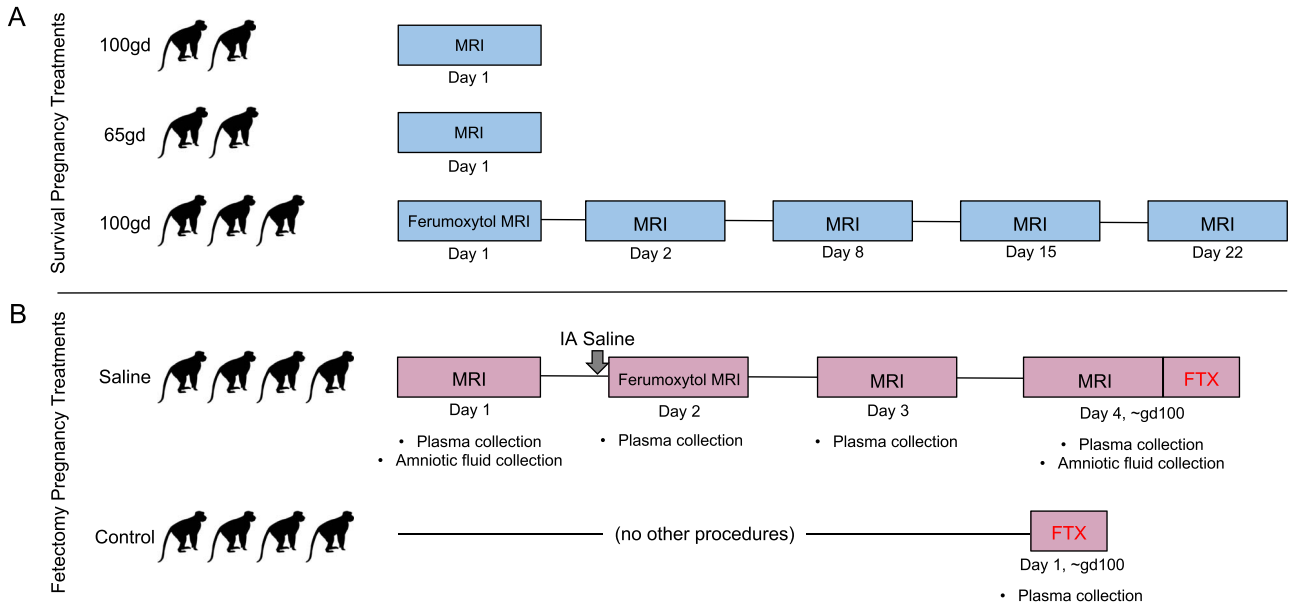

Figure 1. Experimental design. Monkey outlines represent a single animal that received each treatment, represented on their respective timeline. (A) Blue timelines outline experimental design for animals where pregnancy proceeded to term and the infants were born by spontaneous vaginal delivery. (B) Pink timelines outline the series of procedures that animals received whose pregnancies were terminated by fetectomy. IA = intra-amniotic, FTX = fetectomy.

staff in accordance with the regulations and guidelines outlined in the Animal Welfare Act and the Guide for the Care and Use of Laboratory Animals. All animals including infants born from pregnancies that received MRI are systematically monitored twice daily by WNPRC staff and veterinarians, and additionally as needed. All irregular observations are immediately entered into the colony electronic health records. Observations may include the presence of blood, trauma, irregular feces, variation in eating patterns, lethargy, vomit, abnormal behavior including self-injury, evidence of breeding behavior, and infant nursing.

Immune cell isolation and incubation with ferumoxytol

Monocytes and macrophages for in vitro ferumoxytol-uptake studies were isolated from whole blood drawn from 12 pregnant rhesus macaques, at ~100 gestational day (GD) (term = 165GD), as previously reported [25]. Neutrophils were isolated as previously published [26]. All three cell types were incubated in ferumoxytol (Feraheme, AMAG Pharmaceuticals, Waltham, MA) at 0, 50, 100, or 200 μg/ml for 1 h. Additionally, there were incubations of 0 or 200 μg/ml with activating agents (50 ng/ml phorbol-12-myristate-13-acetate (PMA; Sigma-Aldrich, St. Louis, MO)) for all cell types, 750 ng/ml ionomycin (Sigma-Aldrich, St. Louis, MO) for monocytes only). Following incubation, cells were washed and fixed with 2% paraformaldehyde (PFA) for visualization of iron content by Prussian blue staining [27–29]. Cells were imaged using a Nikon Eclipse TE300 microscope with NIS-Elements image capture.

Placental explant incubations in ferumoxytol

Prior to imaging experiments, placental explants were prepared from tissues obtained from untreated animals undergoing fetectomy or cesarean section in unrelated studies, during first trimester of pregnancy ($n = 2$) or at term ($n = 4$). Explants were incubated in ferumoxytol at 0, 100, or 200 μg/ml, diluted in DMEM/F12 with 10% fetal calf serum, for 2, 4, and 24 h at 37 °C in room air/5% CO_2. Explants were fixed in 2% PFA overnight and embedded in paraffin blocks. Tissues were imaged using a Nikon Eclipse TE300 microscope with NIS-Elements image capture.

Prussian blue staining

To visualize cellular iron content, isolated, fixed immune cells grown on coverslips or deparaffinized rehydrated tissue sections were incubated in Prussian blue solution [27–29] for 20 min, washed with deionized water, and mounted with Aquapolymount (Polysciences, Warrington, PA).

MRI impact on pregnancy outcome and postnatal growth

There were two imaging phases in this study. In the first phase (Figure 1A), seven pregnant macaques were imaged, three with ferumoxytol and four without, to establish standard methods for anesthesia and imaging, and to pilot scan settings. These pregnancies went to term after imaging for spontaneous delivery. Animals that did not receive ferumoxytol had a single imaging session and were completed first to determine feasibility and ascertain appropriate imaging sequences prior to the addition of contrast agent. Animals that received ferumoxytol also had four non-ferumoxytol follow-up imaging sessions at ~1 day, 1, 2, and 3 weeks post-ferumoxytol. Infants joined the WNPRC colony and weights of infants exposed to MRI with or without ferumoxytol in-utero were compared to 116 untreated WNPRC 2016 colony infants through their first year of life. Mean and standard deviation weights for untreated colony infants were calculated at different ages, similar to the approach previously published [30]. These experiments were completed before moving to the second phase of the study.

Use of IL-1beta to induce MFI inflammation

In the second phase (Figure 1B), we used a paradigm of ferumoxytol MRI following intra-amniotic injection of 10 mg human recombinant IL-1β (PeproTech, Rocky Hill, NJ) in 0.5 ml sterile saline

($n = 4$). This paradigm has been reported previously to increase decidual macrophage numbers and model chorioamnionitis and preterm labor [31, 32] or sterile saline ($n = 4$), and we used it to test the efficacy of ferumoxytol detection of mononuclear phagocytes and inflammation [17, 20–24] at the MFI. At ~100GD, both saline and IL-1β animals received a baseline MRI without ferumoxytol on day 1, MRI with ferumoxytol on day 2, and follow-up non-ferumoxytol MRIs on days 3 and 4. Untreated controls ($n = 4$) did not receive intra-amniotic injections, ferumoxytol, or MRI. While the resulting R2* maps of the MFI from IL-1β-exposed animals did not differ from those of animals receiving intra-amniotic saline [34], comparison of saline-injected and untreated animals allows determination of any impact of ferumoxytol MRI at the MFI or on the fetus. The results of the IL-1β-exposed animals will not be discussed in this report.

Intra-amniotic injection

Procedures were performed under transabdominal ultrasound guidance on the lateral aspect of the abdomen. A syringe filled with sterile saline was attached to a biopsy needle and inserted through an aseptically prepared site of the abdominal wall until the tip reached the wall of the uterus, avoiding the bowel and bladder ($n = 4$, Figure 1B). The needle was advanced into the amniotic cavity and a small amount of amniotic fluid was drawn to confirm needle placement. The contents of the syringe were then slowly injected into the amniotic cavity, and the needle was withdrawn. Following withdrawal of the needle, the insertion site in the uterus was observed by ultrasound to confirm lack of bleeding.

Magnetic resonance imaging

A total of 11 monkeys were imaged for the current study, seven with ferumoxytol. Experiments took place between January 2016 and April 2018. All animals that underwent an MRI exam, regardless of whether they also received ferumoxytol, were sedated by injection of up to 10 mg/kg ketamine, intubated, and anesthesia was maintained by inhalation of oxygen and 1.5% isoflurane. A pulse oximeter probe was placed and vital signs were monitored every 15 min. Animals were imaged in the right-lateral position and a respiratory bellow was placed around the animal's belly during imaging to enable respiratory-compensated imaging that minimizes motion-related artifacts. Animals that received ferumoxytol had an intravenous catheter placed for injection during imaging.

For scans with ferumoxytol, dynamic contrast enhanced (DCE) images were acquired on a clinical 3.0 T MRI system (Discovery MR750, GE Healthcare, Waukesha, WI) utilizing a 32-channel torso radiofrequency coil (Neocoil, Pewaukee, WI). Time resolved T1-weighted DCE images with 5 s temporal resolution were obtained throughout the ferumoxytol administration [33]. Scanner time for animals that did not undergo DCE scanning, including animal set-up in the magnet and all time between scans, ranged from 1.5 to 2.5 h. Animals that underwent DCE scanning had times ranging from 2 to 4.5 h to do pre- and post-ferumoxytol imaging and calibrations required for DCE. Ferumoxytol diluted 5:1 with normal saline was administered at 4 mg/kg body weight over a 20 s interval using a power injector, followed by a 20 ml saline flush at the same rate. A baseline R2* MRI scan (an MRI relaxation parameter highly correlated and sensitive to detect iron concentration) was performed before ferumoxytol administration. R2* measurements were estimated in the maternal, MFI, and fetal tissues by region-of-interest analysis directly from the MRI images. Follow-up R2* MRI scans were performed on subsequent days after contrast injection to determine the persistence of ferumoxytol in various tissues. MRI acquisition parameter details can be found elsewhere [33, 34].

Assessment of maternal clinical outcomes with ferumoxytol administration

Additional to the seven animals in this study that received MRI with ferumoxytol, one time each, there are several studies not discussed here being completed that also utilize ferumoxytol MRI. Within these studies, there are 28 animals that have received MRI with ferumoxytol up to three times, at the same dose discussed here per imaging session. The seven animals in our current study and these additional 28 animals are considered together to estimate the frequency of potential acute allergic reaction to ferumoxytol. No other information for these additional 28 animals will be considered in this report.

Fetectomy

At ~100GD, the fetoplacental unit was collected via hysterotomy ($n = 8$, Figure 1B). Maternal biopsies were collected aseptically during surgery and the dam recovered. The fetus was euthanized by intravenous or intracardiac injection of 50 mg/kg sodium pentobarbital. Fetal and MFI tissues were dissected for histology, iron content mass spectrometry, and protein assay.

Tissue homogenates

Tissues collected at fetectomy (0.1–0.7 g) (Supplemental Data S1) were homogenized in a Bullet Blender (Next Advance, Troy, NY) at full power for 10 min with non-metal blending beads and 500 µl PBS. Tissue homogenate was stored at −80 °C until use. A 96-well format micro bicinchoninic acid (BCA) protein assay (Thermo Scientific, 23235) was used to determine protein concentrations in homogenates assayed for iron content according to the manufacturer's instructions.

Iron content determinations

Tissue homogenates were assayed for iron concentrations at the Wisconsin State Laboratory of Hygiene Trace Element Research Group in selected maternal, fetal, and MFI tissues via inductively coupled plasma-optical emission spectrometry [35–38]. The limit of detection is 1 µg/g tissue.

Steroid hormone extraction and LC/MS/MS analysis

Maternal plasma samples (450 µl) collected for multi-steroid analysis from animals that had tissues collected at fetectomy (Figure 1B) were extracted and assayed as previously reported [39, 40]. The limit of detection is 30 pg/ml for progesterone; 6 pg/ml for estrone and estradiol.

Histology

Tissues collected for histology were fixed in 4% PFA overnight, 70% ethanol overnight, and routinely processed and embedded in paraffin. About 5 µm sections were stained with H&E and assessed by veterinary pathologists blinded to treatment groups. Tissues were evaluated for the presence or absence of physiologically significant pathologic changes, normal anatomic variations, and inflammation. Morphologic diagnoses (Supplemental Data S2) summarize these histologic findings. Organs not given a morphologic diagnosis

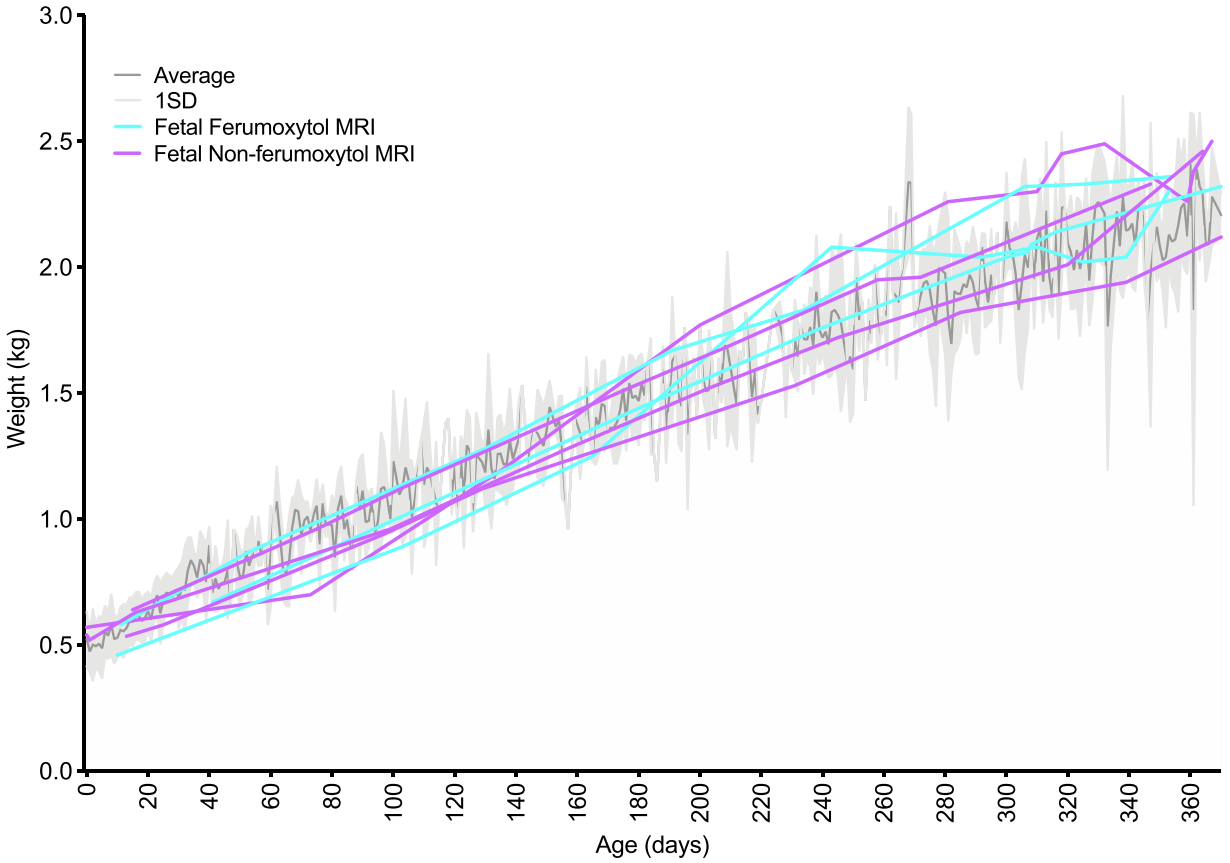

Figure 2. Infant growth rates with maternal ferumoxytol treatment compared to animal colony controls. The dark gray line represents the mean weight (kg) for 116 infants born at the WNPRC in 2016, weighed at the age in days listed on the *x*-axis. The light gray shaded region represents one standard deviation from the mean. Purple lines represent one animal each that was imaged by MRI without ferumoxytol. Aqua lines represent one animal each that was imaged with ferumoxytol, plus four additional scans without additional ferumoxytol administration. The irregular mean and standard deviation lines reflect the fact that not all colony animals were weighted on any given day, so the data represent a different population of animals at any specific time point.

are considered to have no significant pathologic or inflammatory changes and were scored as a 0. Severity (none = 0, minimal = 1, mild = 2, moderate = 3, severe = 4) was determined by the extent and distribution of inflammation, vascular change (infarction, thrombosis, pregnancy associated vascular remodeling, and/or the lack thereof), and non-vascular necrosis across the tissue section or organ (multiple slides were necessary to evaluate the placenta). Scores were averaged and compared between treatment groups as previously reported [41]. Some MFI tissue sections were stained with Prussian blue for iron localization.

Statistics

Iron concentrations in tissue homogenates were compared between treatment groups by 2-way ANOVA and Sidak's multiple comparison test. Differences in pathology and changes in R2* values were assessed by 2-way ANOVA. Hormone level changes were assessed by 1-way ANOVA.

Results

PBMC incubations

To determine whether rhesus macaque cells take up ferumoxytol as reported with human cells [17, 20–24], prior to initiating the imaging phases of this study, rhesus monocytes, macrophages, and neutrophils were incubated in 100 µg/ml ferumoxytol (Supplemental Figure S1), the approximate concentration of ferumoxytol in the blood with administration for MRI, and iron was visualized by Prussian blue staining. Staining was seen in differentiated macrophages but not monocytes or neutrophils. Activation with PMA and ionomycin did not affect iron staining. No staining was seen without ferumoxytol incubation.

Placental explants incubations

To determine whether placental ferumoxytol uptake by placental tissue may confound use for inflammation mapping in vivo, prior to initiating the imaging phases of this study, rhesus placental explants were incubated with ferumoxytol and stained with Prussian blue. Modest background Prussian blue iron staining in tissue was observed independent of ferumoxytol incubation, likely indicating endogenous iron content (Supplemental Figure S2). Minimal increase in iron staining was observed after 2 h of ferumoxytol-incubation. An increase in iron staining appeared after 24 h incubation, specifically in the villous endothelium of the placental tissue. Not substantial staining of the syncytiotrophoblasts was observed, the primary interface exposed to ferumoxytol in maternal blood in vivo. Low levels of endogenous iron and modest increases in ferumoxytol uptake in control placental explants ex vivo after incubations

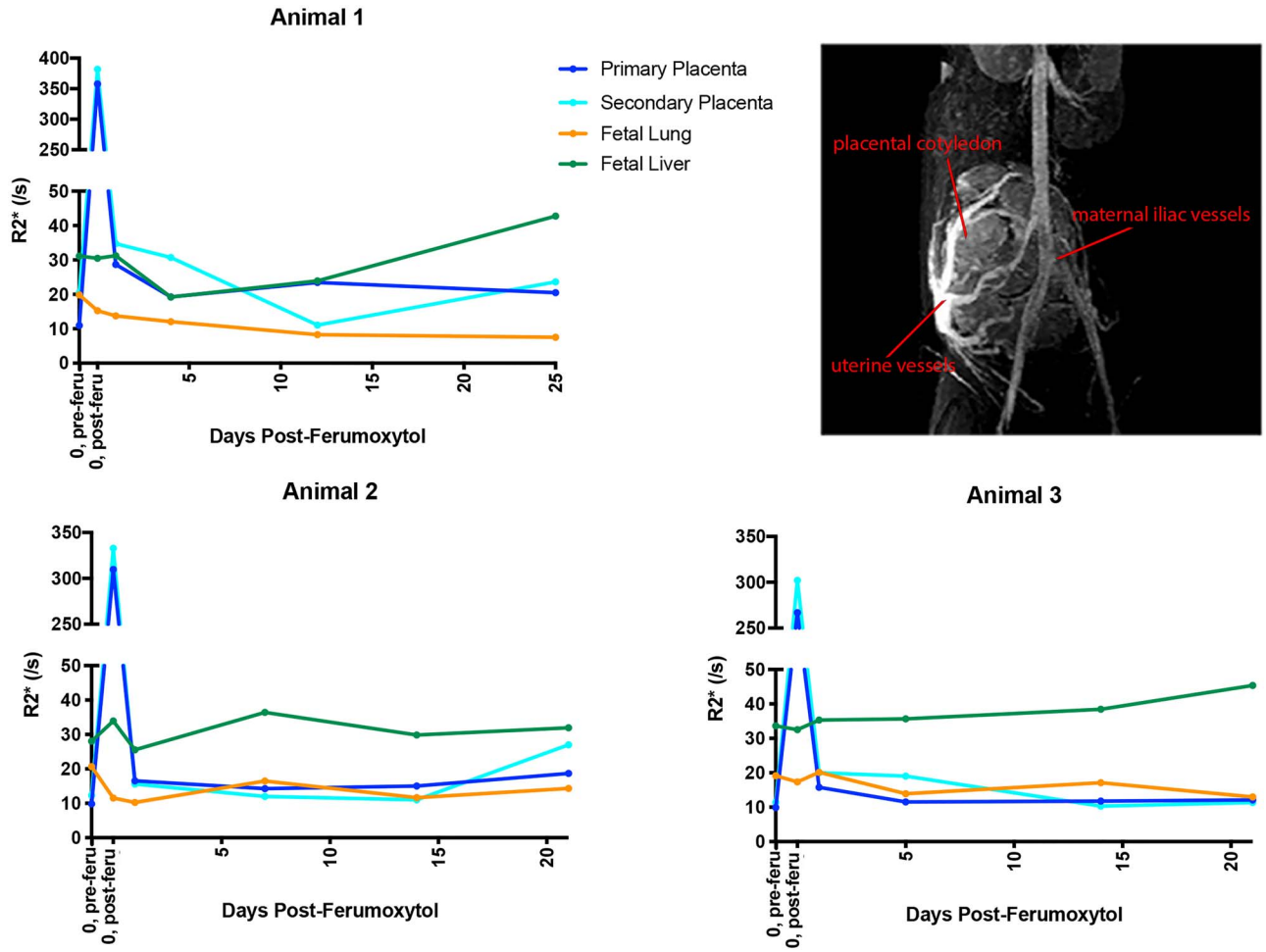

Figure 3. R2* values following ferumoxytol injection. R2* values were monitored in three pregnant rhesus macaques immediately following and 1 day, 1, 2, and 3 weeks ferumoxytol injection. The image on the top right is a representative DCE image of maternal and uterine ferumoxytol detection, including placental intervillous flow, illustrating the imaging data used to determine R2* values. The first point represents pre-injection ("0, pre-feru") and the second point represents the same day post-injection ("0, post-feru"). Primary placental disc values are in dark blue, secondary placenta in aqua, fetal lung in orange, and fetal liver in green.

suggests that in vivo inflammation detection by ferumoxytol-enhanced MRI would be feasible and not confounded by background placental iron content/uptake.

Maternal clinical outcomes with ferumoxytol administration

In addition to the seven animals in this study that received ferumoxytol for MRI (Figure 1), 28 pregnant rhesus monkeys from other ongoing studies (unpublished) had up to three ferumoxytol imaging sessions. In 35 total experimental subjects who had ferumoxytol imaging sessions, two animals required moderate medical attention following ferumoxytol administration. Both animals had periocular edema following IV bolus administration of ferumoxytol that was treated with 10 mg diphenhydramine hydrochloride. One animal had a short period of increased heart rate and SPO2 levels. This animal had previous ocular swelling not associated with ferumoxytol, so it is unclear whether this event was due to ferumoxytol or other drugs used to anesthetize the animal. These mild allergic reactions responded to diphenhydramine and the animals recovered without further medical intervention.

Pregnancy outcomes

Seven pregnant rhesus macaques (Figure 1A) who underwent MRI gave birth via vaginal delivery at term, and the infants joined the WNPRC colony. Results of these imaging studies are described in separate reports [33, 42]. Pregnancy outcomes were generally unremarkable, with one retained placenta (which occurs in ~2.6% of WNPRC pregnancies). None of the seven dams had immediate or long-term reactions to the ferumoxytol treatment.

Infant growth data from these pregnancies are plotted along with their birth year cohort weights (Figure 2). The weights of the MRI offspring generally stayed within one standard deviation of the average infant weights. Infants followed normal physiological and sociobehavioral patterns seen in other colony infants as assessed by daily veterinary observations.

Ferumoxytol detection by MRI following administration

Three of the seven pregnant rhesus macaques that carried infants to term (Figure 1A) had been imaged with ferumoxytol at ~100GD. Imaging occurred immediately before (to establish a baseline R2*

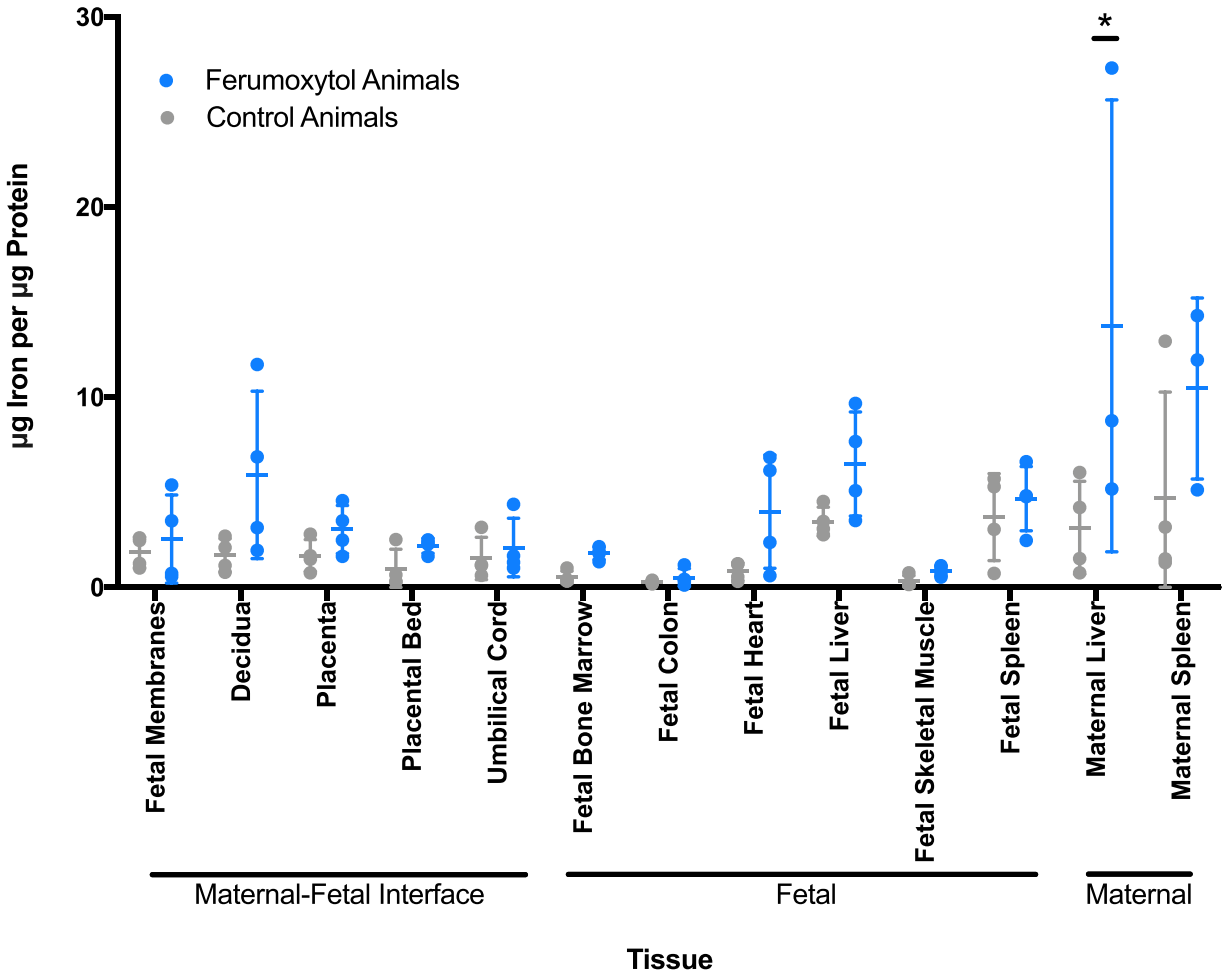

Figure 4. Iron content of maternal and fetal tissues. Iron content of selected tissues was determined by mass spectrometry. Non-imaged animals are represented by gray circles ($n = 4$). Animals that received ferumoxytol imaging with intra-amniotic saline are in blue ($n = 4$, except for maternal liver and maternal spleen where $n = 3$). Mean and standard error are denoted by horizontal lines for each tissue.

values in maternal, MFI, and fetal tissue) and 15 min after administration of ferumoxytol, followed by four follow-up MRI scans at ~1 day, 1, 2, and 3 weeks following ferumoxytol administration. In all three animals, an increase in R2* values in both the primary and secondary placental disks is seen immediately following ferumoxytol injection (Figure 3). The R2* values in fetal lung remained close to baseline though all scans while fetal liver R2* values increased slightly in two of the three animals. This may reflect an increase in physiological iron transport to the fetus over time in normal pregnancy, unrelated to ferumoxytol. The R2* values in the placenta, which increased dramatically following ferumoxytol administration, returned to approximate baseline levels within 1 day post-ferumoxytol, supporting a rapid clearance of ferumoxytol from the blood. Ferumoxytol accumulation in the placenta or transfer to the fetus was not detectable by R2* [34].

Iron content in tissues

Maternal, MFI, and fetal tissues from eight pregnancies (Figure 1B) were surgically collected at ~100GD following MRI and iron concentrations were determined in these tissues (Figure 4). When ferumoxytol-exposed and untreated control groups were compared, only maternal liver showed a significant increase in iron concentration with maternal ferumoxytol administration over control ($P < 0.0001$). There are no significant differences in fetal tissue iron levels in ferumoxytol vs. non-ferumoxytol-exposed animals.

Prussian blue staining of MFI tissues

Prussian blue staining varied animal-to-animal in the placenta, decidua, and fetal membranes from animals that underwent fetectomy. Tissues from ferumoxytol-receiving animals, overall, did not have noticeably different staining compared to non-ferumoxytol-receiving animals. Interestingly, the animal with the most consistent staining had not received ferumoxytol (Supplemental Figure S3), likely reflecting normal physiological iron.

Ferumoxytol effects on plasma progesterone, estrone, and estradiol

For each imaging day in animals that underwent fetectomy (Figure 1B), maternal plasma samples were assessed by mass spectrometry for progesterone, estrone, and estradiol levels [39, 40] to assess the impact of MRI imaging and ferumoxytol administration on placental endocrine function. Non-imaged controls (Figure 1B) received a one-time plasma-collection at time of fetectomy. There

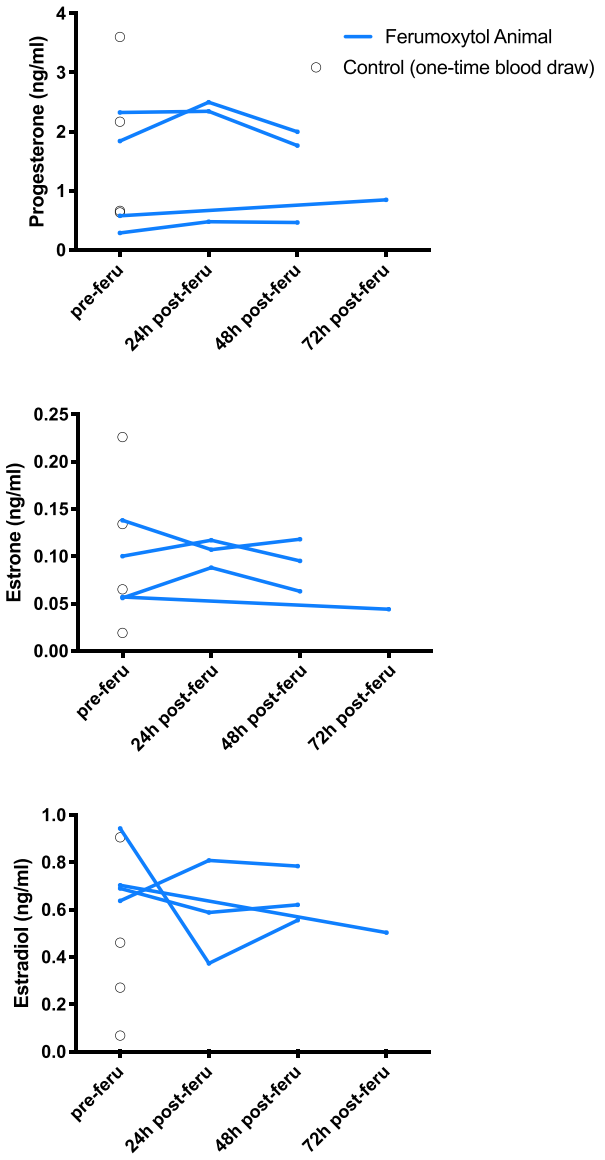

Figure 5. Plasma hormone levels in MRI animals assessed by mass spectrometry. Blue lines represent progesterone, estrogen, and estradiol levels in ferumoxytol-infused animals before injection, 24 h following injection, and 48 or 72 h following injection. Black circles represent single blood draw readings from non-ferumoxytol control animals, indicating the expected range of peripheral blood steroid hormone levels in pregnant macaques.

was no statistically significant change in placental hormone levels following administration of ferumoxytol and hormone levels generally stayed within the range of levels seen in non-imaged controls (Figure 5).

Ferumoxytol effects on histopathology

Of 37 maternal and fetal tissues collected at fetectomy (Supplemental Data S1), the placenta, decidua, amniotic membranes, placental bed, maternal spleen, and maternal liver had notable histopathology. Animals that did and did not receive ferumoxytol MRI had no statistically significant differences in individual tissue histopathology scores (Figure 6). Morphologic diagnoses are provided in Supplemental Data S2.

Discussion

In this study, we examined the impact of MRI with and without ferumoxytol on the fetoplacental and maternal tissues, pregnancy outcomes, and fetal well-being in the pregnant rhesus macaque. Offspring from imaged pregnancies with or without ferumoxytol had uneventful labor and normal growth in comparison with contemporary pregnancies from the WNPRC breeding colony. No significant impact of MRI with ferumoxytol on iron content or histopathology of fetal and MFI tissues (decidua, placenta, fetal membranes) was observed. Placental function as indicated by peripheral blood steroid hormone levels was unaffected by MRI with ferumoxytol. The lack of significant adverse outcomes in the rhesus subjects also suggests the utility of ferumoxytol as a non-gadolinium contrast agent for MRI in pregnancy studies.

In vitro culture experiments demonstrated that ferumoxytol was taken up by macrophages differentiated from peripheral blood monocytes, but not by undifferentiated monocytes or granulocytes. This indicates that ferumoxytol is a feasible reagent to detect the accumulation of phagocytic macrophages at sites of inflammation. Tissue macrophages take up ferumoxytol and clear these iron nanoparticles more slowly than those in the blood, therefore, sites of inflammation can be located by performing delayed imaging following ferumoxytol administration. This paradigm may help identify inflammation at the MFI, which could predict an insult to the pregnancy.

Concerns about ferumoxytol uptake by the placenta and the potential for transport of elevated levels of iron to the fetus, putting the fetus at risk for hemochromatosis or pulmonary hemosiderosis since these disorders result in fetal growth restriction, hepatic failure, alveolar hemorrhage, and stillbirth [43–45] were addressed. Placental villous explants were incubated in vitro with physiologically relevant concentrations of ferumoxytol, and staining of explant tissue sections for iron content with Prussian blue did not demonstrate any significant uptake of SPION by placental tissues in a physiologically meaningful pattern (i.e., syncytiotrophoblast uptake) that would be anticipated with exposure of the placenta to ferumoxytol in the maternal blood in the intervillous space.

The fetus acquires iron during pregnancy through transferrin receptor acquisition of ferritin and transit across the placental syncytiotrophoblast and cytotrophoblast to the fetal vasculature within villous stroma [46]. Placental tissues collected from MRI experiments and stained with Prussian blue for iron content did not reveal discernible differences between tissues from control and ferumoxytol-treated pregnancies. Additionally, decidual tissues and fetal membranes did not demonstrate any consistent differences between experimental groups. There were focally distributed areas of iron detected by Prussian blue staining, however interestingly, the tissues with the clearest demonstration of iron content were the decidua and fetal membranes rather than the placental villi. It is important to note that the animal in which iron was most readily demonstrated in these tissues did not receive ferumoxytol and thus SPION-delivered iron was not the source of Prussian blue staining. These data suggest that although the placenta directly transports iron to the fetus via a biologically conserved ferritin/ferritin receptor-mediated pathway, this active pathway does not participate in the uptake of ferumoxytol by the syncytiotrophoblasts. We hypothesize that cellular iron sequestration, as indicated by Prussian blue staining, may be largely attributable to macrophage uptake of erythrocytes as a routine surveillance function at the MFI.

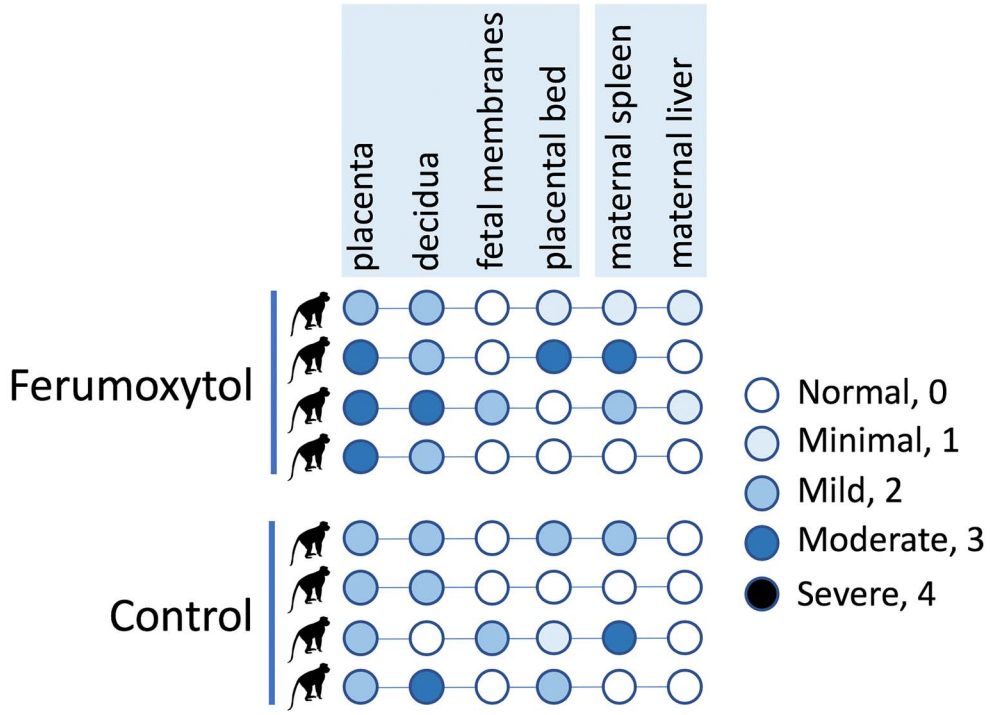

Average Pathology Scores with Standard Error

	Placenta	Decidua	Fetal Membranes	Placental Bed	Maternal Spleen	Maternal Liver
Ferumoxytol	2.75±0.25	2.25±0.25	0.5±0.5	1±0.71	1.5±0.65	0.5±0.29
Control	2±0	1.75±0.63	0.5±0.5	1.25±0.48	1.25±0.75	0±0

Figure 6. Chart summarizing histopathology scores of all tissues that showed pathology. For each animal, the circle representing each tissue is colored to denote severity of pathology. The top four rows represent the ferumoxytol-receiving intra-amniotic saline animals and the bottom four rows are for non-ferumoxytol non-MRI controls. Numbers were assigned to each severity rating and used to analyze pathologies (normal = 0, minimal = 1, mild = 2, moderate = 3, severe = 4). The chart below presents the average pathology scores for each tissue per treatment, used to assess statistical significance.

Consistent with a lack of increase in iron content of MFI tissues by histochemical methods, there was no significant increase in iron concentration in MFI tissues by mass spectrometry. Likewise, fetal tissues that would be anticipated to accumulate iron did not show a statistically significant increase. While there does appear to be a trend for slightly higher, though not statistically significant, iron content in fetal tissues, further studies will be needed to determine if this is a consistent result. There was a statistically significant increase in maternal liver iron content, which was expected since the liver is a main clearance organ for ferumoxytol, with resident hepatic macrophages (Kupffer cells) taking up ferumoxytol particles in studies in rabbit [47] and human subjects [48, 49].

Histopathology was evaluated in selected maternal tissues, the MFI, and in fetal tissues. There was no detectable histopathology in any fetal tissues. While histopathology was noted in tissues at the MFI, there were not significant differences between ferumoxytol-receiving and control animals. Some histopathological features were noted among placentas even in untreated "normal" pregnancies. Functional assessment of the placenta by monitoring of placental hormone secretion (progesterone, estradiol, estrone) likewise revealed no significant difference between animals receiving ferumoxytol MRI imaging, and untreated animals.

The use of an animal model to evaluate MRI methodologies has significant advantages. The pregnant dam is anesthetized for the imaging procedure in the non-human primate model, and the inhaled anesthetic is transferred to the fetus, which is also anesthetized. Therefore, the fetal motion is minimized in MRI of the animals, leading to reliable MRI results. However, anesthesia is not the standard of care for MRI evaluation of pregnant humans and the potential fetal motion in MRI of pregnant human subjects will need to be addressed. A motion-robust R2* mapping technique has been proposed by our group and showed to effectively diminish motion effects in human scans [34]. Upon successful validation, the motion-robust MRI technique may enable detection of macrophage homing in pregnant women. It should also be noted that ferumoxytol was injected as a diluted bolus in our current macaque study, while it is administered as a slow infusion in humans to reduce the risk of anaphylactic reactions.

In summary, we conclude that ferumoxytol administration for imaging in this rhesus pregnancy model is feasible. Ferumoxytol effects on the fetus were minimal in this study with evidence that the SPION may not cross the placenta. Future studies will explore the use of ferumoxytol to detect placental inflammation and the diagnostic value of DCE MRI in the presence of placental dysfunction. The

rhesus macaque will be an important platform for initial development of novel imaging approaches in an experimentally tractable model.

Supplementary data

Supplementary data are available at *BIOLRE* online.

Acknowledgment

The authors wish to thank GE Healthcare who provides research support to the University of Wisconsin-Madison and AMAG Pharmaceuticals for providing Ferumoxytol for this study. Dr Reeder is a Romnes Faculty Fellow, and has received an award provided by the University of Wisconsin-Madison Office of the Vice Chancellor for Research and Graduate Education with funding from the Wisconsin Alumni Research Foundation.

Conflict of interest

The authors have declared that no conflict of interest exists.

References

1. Alexander BT. Placental insufficiency leads to development of hypertension in growth-restricted offspring. *Hypertension* 2003; **41**:457–462.
2. Brosens I, Pijnenborg R, Vercruysse L, Romero R. The "great obstetrical syndromes" are associated with disorders of deep placentation. *Am J Obstet Gynecol* 2011; **204**:193–201.
3. Krishna U, Bhalerao S. Placental insufficiency and fetal growth restriction. *J Obstet Gynaecol India* 2011; **61**:505–511.
4. Roberts DJ, Post MD. The placenta in pre-eclampsia and intrauterine growth restriction. *J Clin Pathol* 2008; **61**:1254–1260.
5. Chalouhi GE, Deloison B, Siauve N, Aimot S, Balvay D, Cuenod CA, Ville Y, Clément O, Salomon LJ. Dynamic contrast-enhanced magnetic resonance imaging: definitive imaging of placental function? *Semin Fetal Neonatal Med* 2011; **16**:22–28.
6. Lohrke J, Frenzel T, Endrikat J, Alves FC, Grist TM, Law M, Lee JM, Leiner T, Li KC, Nikolaou K, Prince MR, Schild HH et al. 25 years of contrast-enhanced MRI: developments, current challenges and future perspectives. *Adv Ther* 2016; **33**:1–28.
7. Frias AE, Schabel MC, Roberts VH, Tudorica A, Grigsby PL, Oh KY, Kroenke CD. Using dynamic contrast-enhanced MRI to quantitatively characterize maternal vascular organization in the primate placenta. *Magn Reson Med* 2015; **73**:1570–1578.
8. Schabel MC, Roberts VHJ, Lo JO, Platt S, Grant KA, Frias AE, Kroenke CD. Functional imaging of the nonhuman primate placenta with endogenous blood oxygen level-dependent contrast. *Magn Reson Med* 2016; **76**:1551–1562.
9. Siauve N, Chalouhi GE, Deloison B, Alison M, Clement O, Ville Y, Salomon LJ. Functional imaging of the human placenta with magnetic resonance. *Am J Obstet Gynecol* 2015; **213**:S103–S114.
10. Ray JG, Vermeulen MJ, Bharatha A, Montanera WJ, Park AL. Association between MRI exposure during pregnancy and fetal and childhood outcomes. *JAMA* 2016; **316**:952–961.
11. Rogosnitzky M, Branch S. Gadolinium-based contrast agent toxicity: a review of known and proposed mechanisms. *Biometals* 2016; **29**:365–376.
12. Oh KY, Roberts VH, Schabel MC, Grove KL, Woods M, Frias AE. Gadolinium chelate contrast material in pregnancy: fetal biodistribution in the nonhuman primate. *Radiology* 2015; **276**:110–118.
13. Prola-Netto J, Woods M, Roberts VHJ, Sullivan EL, Miller CA, Frias AE, Oh KY. Gadolinium chelate safety in pregnancy: barely detectable gadolinium levels in the juvenile nonhuman primate after in utero exposure. *Radiology* 2018; **286**:122–128.
14. Kanal E, Barkovich AJ, Bell C, Borgstede JP, Bradley WG, Froelich JW, Gimbel JR, Gosbee JW, Kuhni-Kaminski E, Larson PA, Lester JW, Nyenhuis J et al. ACR guidance document on MR safe practices: 2013. *J Magn Reson Imaging* 2013; **37**:501–530.
15. AMAG Pharma. *Feraheme: Highlights of Prescribing Information [Internet]*; 2018. https://www.accessdata.fda.gov/drugsatfda_docs/label/2009/022180lbl.pdf. Accessed 2 August 2020.
16. Auerbach M, Landy HJ. *Anemia in pregnancy [Internet]. UpToDate*; 2019. https://www.uptodate.com/contents/anemia-in-pregnancy?topicRef=7148&source=see_link. Accessed 2 August 2020.
17. Bashir MR, Bhatti L, Marin D, Nelson RC. Emerging applications for ferumoxytol as a contrast agent in MRI. *J Magn Reson Imaging* 2015; **41**:884–898.
18. Knobloch G, Colgan T, Wiens CN, Wang X, Schubert T, Hernando D, Sharma SD, Reeder SB. Relaxivity of Ferumoxytol at 1.5 T and 3.0 T. *Investig Radiol* 2018; **53**:257–263.
19. Ludwig KD, Fain SB, Adamson EB, Nguyen S, Golos TG, Reeder SB, Bird IM, Wieben O, Shah DM, Johnson KM. Quantitative ferumoxytol DCE MRI of the primate placental perfusion domains. In: *Proceedings from the 26th Annual Meeting of ISMRM*. Paris, France; 2018.
20. Toth GB, Varallyay CG, Horvath A, Bashir MR, Choyke PL, Daldrup-Link HE, Dosa E, Finn JP, Gahramanov S, Harisinghani M, Macdougall I, Neuwelt A et al. Current and potential imaging applications of ferumoxytol for magnetic resonance imaging. *Kidney Int* 2017; **92**:47–66.
21. Hasan DM, Amans M, Tihan T, Hess C, Guo Y, Cha S, Su H, Martin AJ, Lawton MT, Neuwelt EA, Saloner DA, Young WL. Ferumoxytol-enhanced MRI to image inflammation within human brain arteriovenous malformations: a pilot investigation. *Transl Stroke Res* 2012; **3**:166–173.
22. Iv M, Samghabadi P, Holdsworth S, Gentles A, Rezaii P, Harsh G, Li G, Thomas R, Moseley M, Daldrup-Link HE, Vogel H, Wintermark M et al. Quantification of macrophages in high-grade gliomas by using ferumoxytol-enhanced MRI: a pilot study. *Radiology* **2018**:181204.
23. Neuwelt A, Sidhu N, Hu CA, Mlady G, Eberhardt SC, Sillerud LO. Iron-based superparamagnetic nanoparticle contrast agents for MRI of infection and inflammation. *AJR Am J Roentgenol* 2015; **204**:W302–W313.
24. Gaglia JL, Harisinghani M, Aganj I, Wojtkiewicz GR, Hedgire S, Benoist C, Mathis D, Weissleder R. Noninvasive mapping of pancreatic inflammation in recent-onset type-1 diabetes patients. *Proc Natl Acad Sci U S A* 2015; **112**:2139–2144.
25. Rozner AE, Dambaeva SV, Drenzek JG, Durning M, Golos TG. Generation of macrophages from peripheral blood monocytes in the rhesus monkey. *J Immunol Methods* 2009; **351**:36–40.
26. Roberts RL, Gallin JI. Rapid method for isolation of normal human peripheral blood eosinophils on discontinuous Percoll gradients and comparison with neutrophils. *Blood* 1985; **65**:433–440.
27. Sheehan D, Hrapchak B. *Theory and Practice of Histotechnology*, 2nd ed. Ohio: Battelle Press; 1980: 217–218.
28. Luna L. *Manual of Histologic Staining Methods of the AFIP*, 3rd ed. NY: McGraw-Hill; 1968: 183.
29. Crookham J, Dapson R. *Hazardous Chemicals in the Histopathology Laboratory*, 2nd ed. Battle Creek, Michigan: Anatech; 1991.
30. Tarantal AF. Ultrasound imaging in rhesus (*Macaca mulatta*) and long-tailed (*Macaca fascicularis*) macaques: reproductive and research applications. In: Wolfe-Coote S (ed.), *The Laboratory Primate*. London: Elsevier; 2005: 317–352.
31. Presicce P, Senthamaraikannan P, Alvarez M, Rueda CM, Cappelletti M, Miller LA, Jobe AH, Chougnet CA, Kallapur SG. Neutrophil recruitment and activation in decidua with intra-amniotic IL-1beta in the preterm rhesus macaque. *Biol Reprod* 2015; **92**:56.
32. Kallapur SG, Presicce P, Senthamaraikannan P, Alvarez M, Tarantal AF, Miller LM, Jobe AH, Chougnet CA. Intra-amniotic IL-1β induces fetal inflammation in rhesus monkeys and alters the regulatory T cell/IL-17 balance. *J Immunol* 2013; **191**:1102–1109.

33. Ludwig KD, Fain SB, Nguyen SM, Golos TG, Reeder SB, Bird IM, Shah DM, Wieben OE, Johnson KM. Perfusion of the placenta assessed using arterial spin labeling and ferumoxytol dynamic contrast enhanced magnetic resonance imaging in the rhesus macaque. *Magn Reson Med* 2018; **81**:1964–1978.
34. Zhu A, Reeder SB, Johnson KM, Nguyen SM, Golos TG, Shimakawa A, Muehler MR, Francois CJ, Bird IM, Fain SB, Shah DM, Wieben O et al. Evaluation of a motion-robust 2D chemical shift-encoded technique for R2* and field map quantification in ferumoxytol-enhanced MRI of the placenta in pregnant rhesus macaques. *J Magn Reson Imaging* 2019. epub ahead of print. doi: 10.1002/mrm.27876.
35. Krynitsky AJ. Preparation of biological tissue for the determination of arsenic and selenium by graphite furnace atomic absorption spectrometry. *Anal Chem* 1987; **59**:1884–1886.
36. Giesy JP, Wagner JG. Frequency distributions of trace metal concentrations in five freshwater fishes. *Trans Am Fish Soc* 1977; **1064**: 393–403.
37. Test Methods for Evaluating Solid Waste Physical/Chemical Methods, 3rd ed. SW-846, USEPA. November 1986, including July 1992, August 1993, September 1994, and January 1995 updates. Method 6010B.
38. Methods for the Determination of Metals in Environmental Samples, Supplement I. EPA-600/R-94/111. Cincinnati, Ohio: Environmental Monitoring Systems Laboratory, USEPA. May 1994; Method 200.7.
39. Kenealy BP, Kapoor A, Guerriero KA, Keen KL, Garcia JP, Kurian JR, Ziegler TE, Terasawa E. Neuroestradiol in the hypothalamus contributes to the regulation of gonadotropin releasing hormone release. *J Neurosci* 2013; **33**:19051–19059.
40. Kenealy BP, Keen KL, Kapoor A, Terasawa E. Neuroestradiol in the stalk median eminence of female rhesus macaques decreases in association with puberty onset. *Endocrinology* 2016; **157**:70–76.
41. Nguyen SM, Antony KM, Dudley DM, Kohn S, Simmons HA, Wolfe B, Salamat MS, Teixeira LBC, Wiepz GJ, Thoong TH, Aliota MT, Weiler AM et al. Highly efficient maternal-fetal Zika virus transmission in pregnant rhesus macaques. *PLoS Pathog* 2017; **13**:e1006378.
42. Macdonald JA, Corrado PA, Nguyen SM, Johnson KM, Francois CJ, Magness RR, Shah DM, Golos TG, Wieben O. Uteroplacental and fetal 4D flow MRI in the pregnant rhesus macaque. *J Magn Reson Imaging* 2018; **49**:534–545.
43. Kelly AL, Lunt PW, Rodrigues F, Berry PJ, Flynn DM, McKiernan PJ, Kelly DA, Mieli-Vergani G, Cox TM. Classification and genetic features of neonatal haemochromatosis: a study of 27 affected pedigrees and molecular analysis of genes implicated in iron metabolism. *J Med Genet* 2001; **38**:599–610.
44. Fellman V, Rapola J, Pihko H, Varilo T, Raivio KO. Iron-overload disease in infants involving fetal growth retardation, lactic acidosis, liver haemosiderosis, and aminoaciduria. *Lancet* 1998; **351**:490–493.
45. Limme B, Nicolescu R, Misson JP. Neonatal pulmonary hemosiderosis. *Case Rep Pediatr* 2014; **2014**:463973.
46. Fuchs R, Ellinger I. Endocytic and transcytotic processes in villous syncytiotrophoblast: role in nutrient transport to the human fetus. *Traffic* 2004; **5**:725–738.
47. Yancy AD, Olzinski AR, Hu TC, Lenhard SC, Aravindhan K, Gruver SM, Jacobs PM, Willette RN, Jucker BM. Differential uptake of ferumoxtran-10 and ferumoxytol, ultrasmall superparamagnetic iron oxide contrast agents in rabbit: critical determinants of atherosclerotic plaque labeling. *J Magn Reson Imaging* 2005; **21**:432–442.
48. Lim JH, Choi D, Cho SK, Kim SH, Lee WJ, Lim HK, Park CK, Paik SW, Kim YI. Conspicuity of hepatocellular nodular lesions in cirrhotic livers at ferumoxides-enhanced MR imaging: importance of Kupffer cell number. *Radiology* 2001; **220**:669–676.
49. Ramanathan RK, Korn RL, Raghunand N, Sachdev JC, Newbold RG, Jameson G, Fetterly GJ, Prey J, Klinz SG, Kim J, Cain J, Hendriks BS et al. Correlation between ferumoxytol uptake in tumor lesions by MRI and response to nanoliposomal irinotecan in patients with advanced solid tumors: a pilot study. *Clin Cancer Res* 2017; **23**:3638–3648.